Axial seal for high-rpm application and poor lubrication

Christoph Schüle, M.Sc., Dipl.-Ing. (FH) Martin Franz, Dr.-Ing. Christoph Wehmann, Sergio Amorim, M.Sc. Trelleborg Sealing Solutions Germany GmbH, Stuttgart, Germany

1 Introduction

The electrification of drivetrains brings big advantages for users of vehicles and the surrounding environment. However, component suppliers will experience drastic reductions of product variety due to reduced complexity of electrified drivetrains. Current estimations are suggesting that the automotive market alone, aside from all other transportation equipment, will demand in the range of 11 million new pure electrically driven light vehicles by 2025. /1/

A major technology in electric vehicles is the electric drive unit, a combined electric motor and gearbox that fits within the traditional axle/differential space. The motor and gearbox are directly coupled but while the gearbox requires efficient lubrication, it is essential that the motor remains dry and so a highly reliable sealing solution is required between these two components. Electric motors run most efficiently at high speeds and so the seal requirements are very different from those for a transmission input on a combustion engine vehicle – the speeds are a lot higher; the duty cycle is much more varied and there is a reversing requirement. *(The main pain points with regards to the seal are the fact that rotary seal and bearings are limiting factors for the electric motor performance, friction and torque of the seal cause high power losses and active cooling of sealing and bearing might have a need of complex cooling setup with for example additional oil pumps.)*

2 State of the Art

Sealing system of a typical automotive application needs a lifetime of nearly 14 years. /2/ During this lifetime the sealing behavior should be as constant as possible in different operation points which are defined by speed, lubrication and temperature, amongst others. The following chapter gives a short introduction in state of the art radial and axial sealing solution and their influence on power loss.

2.1 Rotary Lip Seals

Most common to seal a rotating shaft against a fluid are rotary lip seals made of elastomer or PTFE. Different subtypes of this seals were developed in the last decades. They all have in common that these types of seals are running on the same track and generate power loss – especially while poor lubricated and higher coefficient of friction μ.

The power loss P of a seal can be estimated according to /3/:

$$P = \mu \cdot p \cdot v \cdot \pi \cdot D \cdot b \qquad (1)$$

This formula describes in a first approximation a linear relationship between power loss and surface velocity. This power loss leads to an increased contact temperature that is finally depending on the heat transfer. There are different models to calculate the temperature in the seal contact. For elastomer seals Engelke /4/ is providing a recursive model to calculate the contact temperature.

More advanced is the IMA ExACT equation that includes e.g., filling level to improve the contact temperature prediction of an elastomer seal. First results show also a good accordance with PTFE lip seals with adapted parameters. /5/

In practice, this mechanism leads to defects of the sealing edge, oil coal, shaft run-in and material degradation. /6/

2.2 Elastomer Axial seals

Another possibility to seal a rotating shaft is an axial elastomer seal, also called V-Ring. This sealing element is rotating on the shaft and has a dynamic load that is comparatively high compared to radial oil seals. Axial seals are known for many decades and show a different behavior with increasing rotational velocity compared to radial seals.

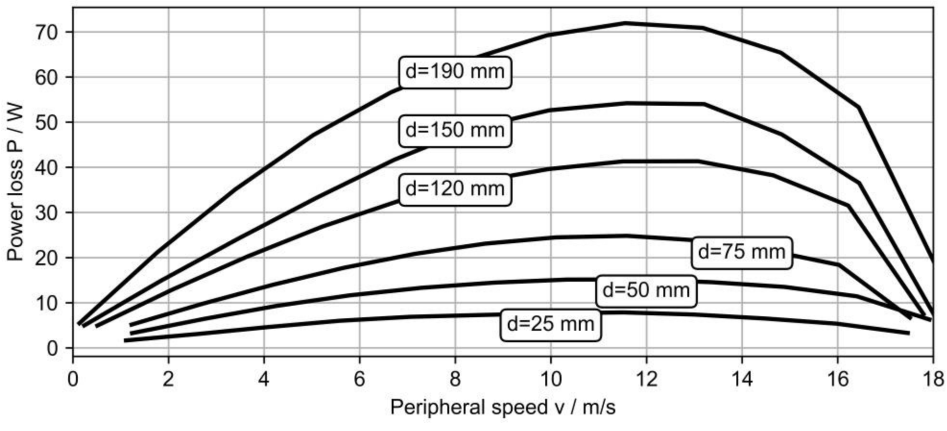

Figure 1 Power loss V-Ring NBR general use (N6T50) based on /7/

Axial elastomer seals are in use for poor lubricated or dry-running applications. An unlubricated elastomer metal contact can lead to a higher wear and with increased circumferential speed the elastomer lip is to certain extent uncontrolled. Furthermore, the seal is moving on elliptical path while accelerating or decelerating. Going in contact means in this case that the interaction area is constantly undefined. The described mechanism was simulated with an axisymmetric model and a hyperelastic material. The shore hardness of the used NBR is 65 Shore A. The deformation and normal force of the seal are shown in Figure 2. While the left picture shows the situation after the installation, the picture in the middle is at 4000 rpm (10.5 m/s) and the picture on the right side the situation at 7000 rpm (18.3 m/s) with no more interaction between counter surface and seal.

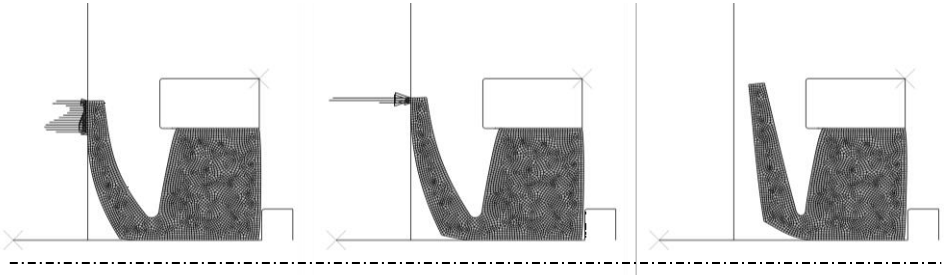

Figure 2 FEA V-Ring

3 Proposed solution

In chapter 2 it was shown that especially radial seals have the disadvantage with an increased power loss at higher speeds and in addition a poor lubrication leads to a reduced lifetime. Instead, axial elastomer seals have a decreasing power loss at higher speeds but have problems with the instability of the sealing lip and elastomer-metal contact.

Thus, the presented design tries to combine the advantages of an axial seal with a PTFE contact. In addition, the contact area is moving perpendicular to the counter surface to have a defined contact zone. Additionally, the design leads to a load-dependent adjustment of the contact force

3.1 Design

The geometric key element of the design are spatial structures around the circumference. These spatial structures work as a deformation reserve when activated by a centrifugal force. The principal is described in Figure 3.

On the left side the three-dimensional structures are static and not activated. For the applications it means the shaft is standing or rotating with limited rotational speed. Thus, the centrifugal force is insufficient to move the structures.

On the right side of Figure 3 the spatial structures are activated and moving in radial direction. This leads to an axial pulling force which reduces the contact force. The forces and deformation are depending on the ratio of material’s density, design and modulus or rather stress-strain curve.

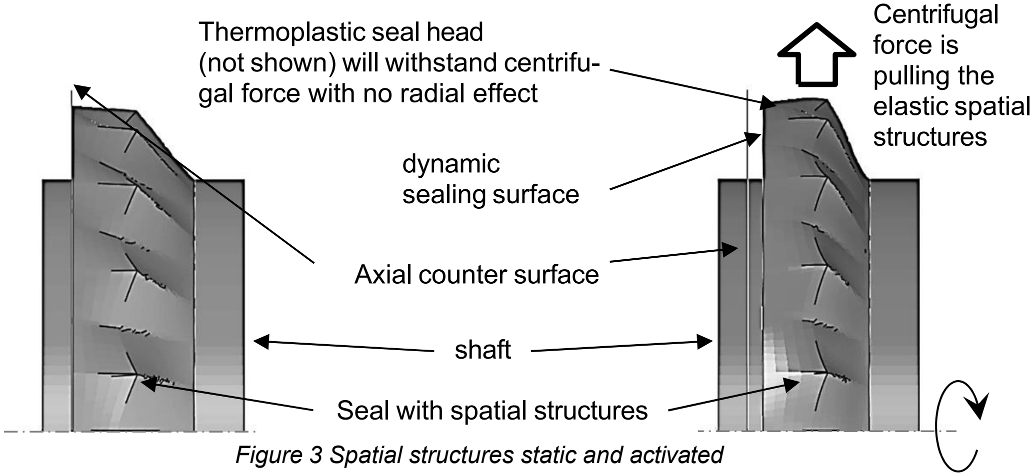

Figure 3 Spatial structures static and activated

The proposed solution is a multicomponent axial seal with the following components, shown in Figure 4:

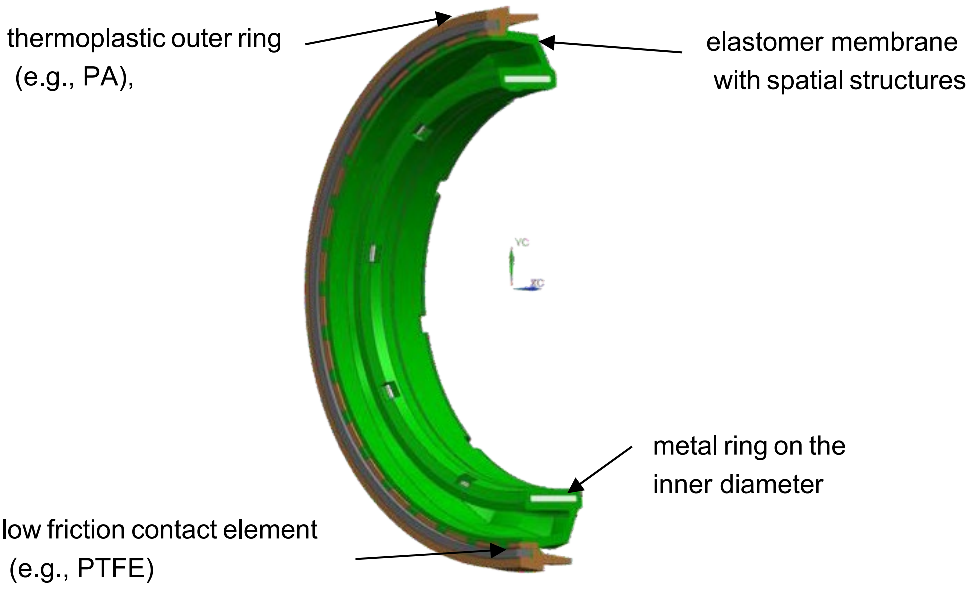

Figure 4 Axial seal design

The seal is fixed on the shaft and running against the counter surface. The axial deformation of the membrane leads to an initial contact force. Thus, the seal is statically tight. By rotational movement, the special membrane design uses the centrifugal force to start an axial movement of the outer ring and the contact element. Due to movement the contact force will be reduced, and the seal is a kind of self-protecting for increased circumferential speed.

The structures in combination with the outer ring, lead to an axial movement and allows the contact element to be nearly perpendicular to the counter surface and avoid moving on a circular path. In the presented design the outer ring is the radial limitation for the membrane movement and provides a groove for the contact element. The contact element is made of a PTFE compound. To improve the performance the material can be adapted to media and counter surface. Also using the outer ring using as a dynamic sealing area is possible.

Compared to radial seals the static eccentricity and dynamic shaft run-out are not critical due to the design. Instead, the eccentricity of the inner and outer ring is important to avoid imbalances.

For increasing speeds, the medium will be splashed away by the thermoplastic part of the rotating seal. This leads to a reduced amount of fluid in the sealing area, when the contact force is reduced.

3.2 Simulation

The simulation of the proposed design was performed in the software Abaqus. The quasi-static simulation was used to simulate different operating points. The parts of the seal were defined as deformable bodies, while counter surface and shaft were defined as rigid bodies. The shaft diameter in the simulation was 50 mm.

The membrane and the thermoplastic head were meshed with tetrahedral elements, while the metal ring and the contact element were meshed with hexahedral elements. The FKM elastomer was modeled with a hyperelastic material model. The shore hardness is 70 Shore A. The thermoplastic part was modeled as a polyamide with an elastic material behavior, while for the low-friction part a PTFE with elastic-plastic material model was used. The metal ring was defined as a steel part. μ between PTFE and counter surface was estimated constant with 0.1. The shown simulation is not including anisotropic material behavior or misalignments between metal and thermoplastic ring, both leading to dynamic unbalance.

Figure 5 shows the displacement in three different stages. On the left side the seal is assembled and axially compressed. In the middle the seal is rotating with 7000 rpm (18.3 m/s) and the spatial structures of the membrane show a radial displacement in the softer membrane areas. The right side of the picture shows the activation of the membrane at 15000 rpm (39.3 m/s). The elastomer part is moving in radial direction and the movement is limited by the thermoplastic head. The thermoplastic head shows also a radial movement bigger than 0.1 mm. The sealing lip lifts off at approximately 12500 rpm (32.7 m/s), hence, from this speed on a small gap exists there.

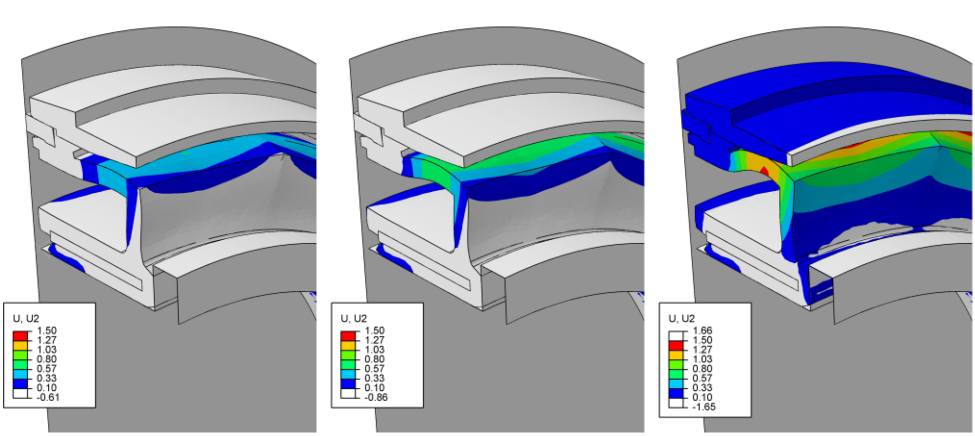

Figure 5 Radial deformation (U2) in different operation points

While Figure 5 shows the deformation in mm including movements of parts by boundary conditions, Figure 6 shows the material specific strain. The logarithmic strain shows also the areas giving flexibility. In addition, it shows the areas with the highest load and most critical areas in transition area of the shaft area and the membrane.

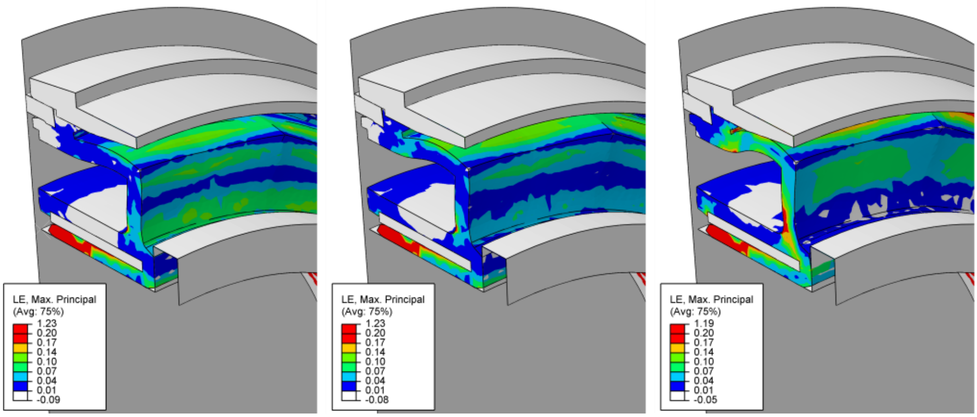

Figure 6 Logarithmic strain in different operation points

In general, the rotation of an axial seal leads to a radial flow and this effect can be used to establish a sealing function. As mentioned the seal lifts up at approx. 12500 rpm and from then on a leakage gap exists. However, due to the radial fluid flow which occurs due to the rotation, the sealing system still can maintain zero leakage, even if there is a small gap between the seal and the countersurface. To guarantee no leakage at all rotation speeds, the radial flow needs to be sufficient at the lift off rotation speed.

A “critical speed” exists at which the radial flow reasoned by centrifugal forces and the flow reasoned by the external pressure are in balance. Above this critical speed, no leakage will occur, even if there is a gap due to the lift-off. In order to design the seal in the way that it lifts above this critical speed, an analytical fluid calculation was carried out. An analytical procedure was chosen because it allows easy understanding of the general influence of the parameters of the design.

In order to develop an analytical model, some simplifications are necessary. Figure 7 provides an overview of the design and the relevant design parameters. The sealing gap has the dimensions w and h. In this area, the flow is considered in the following.

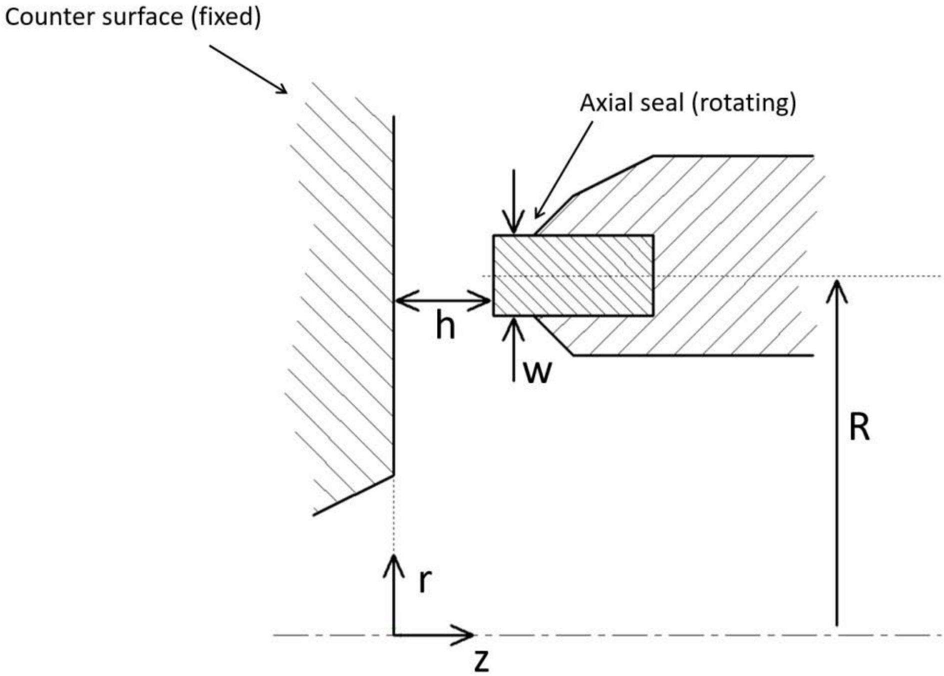

Figure 7: Overview over simplified model and design parameters

First, a simple flow in tangential direction is considered which is reasoned by the rotation of the seal. Accordingly, it is assumed that $u_r = u_z = 0$ holds. The required Navier-Stokes equations in cylinder coordinates are for example provided by Landau and Lifschitz /8/. Simplifying the Navier-Stokes equations and capturing the boundary conditions leads to the following flow in tangential direction.

$$u_\varphi = \frac{\omega}{h} r z \tag{2}$$

Where ω is the angular velocity, given by the rpm through $\omega = 2 \pi n$. The corresponding pressure field is given by equation (3). In this equation, p_i is the pressure at the inner diameter and R_i is the inner radius. Furthermore, ρ is the density.

$$p = p_i + \frac{1}{2} \frac{\rho \omega^2}{h^2} (r^2 - R_i^2) z^2 \tag{3}$$

The pressure is built up by the centrifugal forces and as expected, its maximum is located at the outer diameter and the rotating part of the seal. The corresponding point is $(r, z) = (R_a, h)$.

Next, the pressure given by (3) is used as an input to a pressure driven flow in radial direction. Simplifying the Navier-Stokes equations by assuming $R \gg w$ and $u_\varphi = u_z = 0$, the following general solution for the flow can be obtained, compare Spurk and Aksel /9/. Of course, assuming $u_\varphi = 0$ conflicts the first assumption we used to obtain equation (3). However, since we are interested in the critical speed, this conflict is acceptable because it vanishes at the critical speed. It vanishes because the radial flow will become zero at the critical speed.

$$u_r = \frac{K\,h^2}{2\,\eta}\,(1 - \frac{z}{h})\,\frac{z}{h} \tag{4}$$

In (4) η is the viscosity of the fluid and K is a constant given by the pressure gradient:

$$K = \frac{\partial p}{\partial r} \tag{5}$$

Finally, the fluid flow becomes (6). We introduced the pressure $\tilde{p}_a$ which is a reduced pressure. The idea behind the pressure reduction is that the pressure given by equation (3) is acting against the pressure p_a which is acting on the seal.

$$u_r = \frac{\tilde{p}_a - p_i}{R_i - R_a}\,\frac{h^2}{2\,\eta}\,(1 - \frac{z}{h})\,\frac{z}{h} \tag{6}$$

The reduced pressure can be calculated as described below.

$$\begin{aligned}\tilde{p}_a &= p_a - \Delta p(r = R_a, z = \xi h) \\ &= p_a - \frac{1}{2}\frac{\rho\,\omega^2}{h^2}\,({R_a}^2 - {R_i}^2)\,\xi^2 h^2\end{aligned} \tag{7}$$

Here, ξ defines an average pressure reduction. Its value can be between 0 and 1 – accordingly it takes the pressure from equation (3) between its extreme values.

Finally, the radial flow becomes

$$u_r = \frac{1}{R_i - R_a}\{p_a - p_i - \frac{1}{2}\frac{\rho\,\omega^2}{h^2}\,({R_a}^2 - {R_i}^2)\,\xi^2 h^2\}\,\frac{h^2}{2\,\eta}\,(1 - \frac{z}{h})\,\frac{z}{h} \tag{8}$$

It has a negative value because if leakage occurs, the flow will occur in negative radial direction. The integral of this equation provides the volume flow. In equation (9) its absolute value is shown.

$$|V| = \iint_A |u_r|\,dA = \frac{h^3}{6\,\eta}\,\frac{\pi\,R}{R_a - R_i}\,\{p_a - p_i - \frac{1}{2}\rho\,\omega^2\,\xi^2\,({R_a}^2 - {R_i}^2)\} \tag{9}$$

The critical speed is reached when no leakage occurs, hence, $V = 0$ holds. In the following, the parameters of the developed seal are used in order to estimate the critical speed. Figure 8 shows the resulting mass flow $\dot{m} = \rho\,V$.

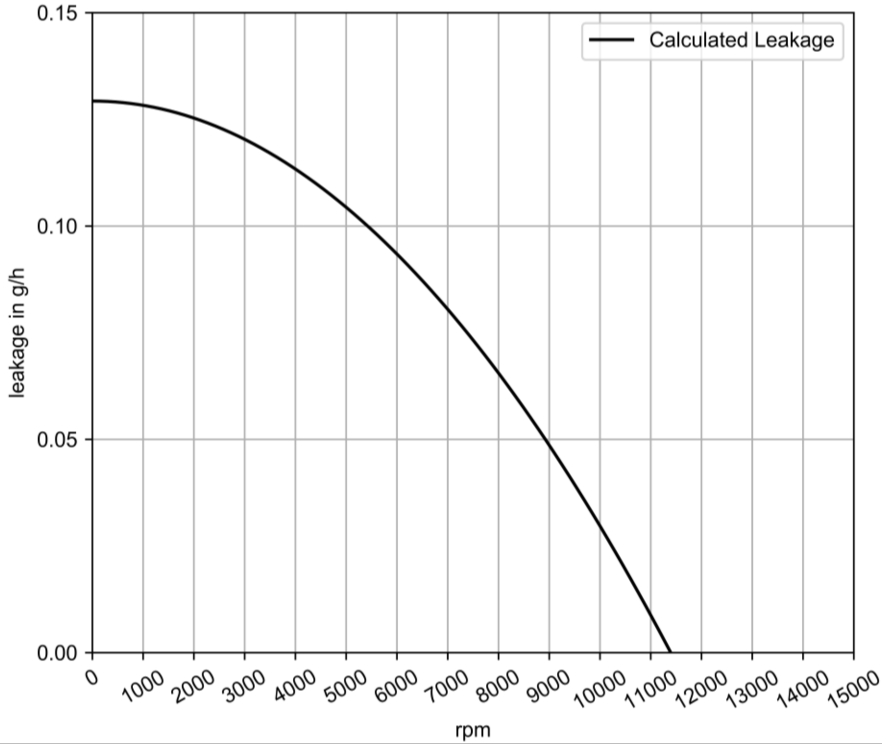

Figure 8: Leakage through sealing gap and estimation of critical speed

The critical speed is at approximately 11000 rpm. As the FEA results showed, this is below the lift-off and therefore, at lower speeds zero leakage is guaranteed, too.

4 Experimental Results

4.1 Test procedure

First tests of the shown seal design were performed on a dedicated high-speed test rig under dry conditions. In a first stage the seal was tested with a stepped stair-like load spectrum. The nominal shaft diameter in the test was 50 mm and in the test was performed for 1000 h by repeating the load spectrum. The step-by-step load spectrum can be split in four areas with different substeps:

- Area I: Low speed up to 2000 rpm (5.2 m/s)
- Area II: Medium speed 2000 rpm to 7000 rpm (18.3 m/s)
- Area III: High speed 7000 rpm to 11000 rpm (28.8 m/s)
- Area IV: Very high speed 11 000 rpm to 15 000rpm (39.3 m/s)

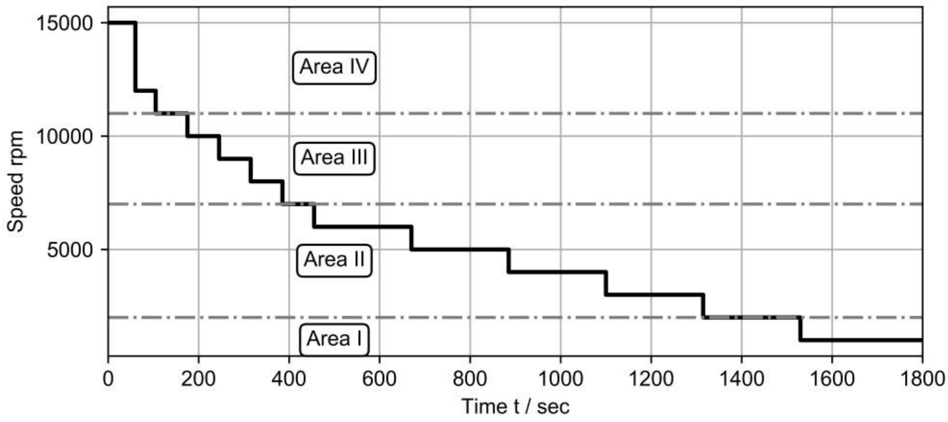

Figure 9 Load spectrum

The hold time in every area was defined by experience and market observation in the automotive sector. In a first approach, the percent share is comparable to a typical load spectrum of a car. The stepwise test with different operating points allows a comparison over time and to draw a conclusion on wear. During the test, data, e.g., rpm, torque, were measured and recorded for further investigations.

4.2 Test results

The seal was assembled with a pretension of 1.6 mm and was running dry under room temperature. The tightness was tested manually by spraying oil on the sealing contact. This procedure was repeated six times during the test and showed no leakage.

The generated data in the test are used to compare simulation with the test result. To compare the simulated axial reaction force with the measured torque following equation was used:

$$M = \mu \ \frac{D_m}{2}\ F_r \qquad (10)$$

While D_m describes the average diameter of the PTFE element and F_r the calculated reaction force.

Figure 10 shows the comparison of test and simulation. The test results are the average torque in the operating points described in 4.1. The average is calculated over the first 72 h of test or 144 iterations of the load spectrum.

The predicted and calculated results show similar curve characteristics, while the predicted curve with μ=0.1 underestimates the test results in a wide range of the application. Due to the fact, that μ has no influence on the axial relief the conversion between simulation and test can be calculated with μ=0.2. This curve shows a good correlation between 3000 rpm (7.9 m/s) and 12000 rpm (31.4 m/s).

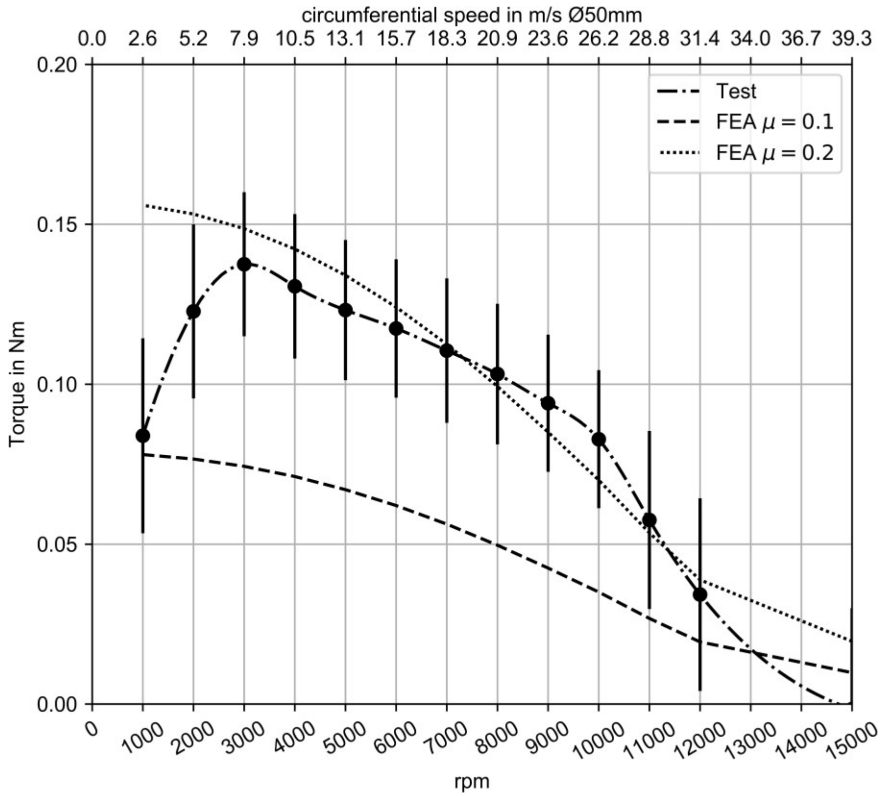

Figure 10 Test results and comparison FEA

Figure 7 shows the assembled seal after the test. The pretensioned spatial structures are still visible and indicate that the PTFE is still in contact with the counter surface.

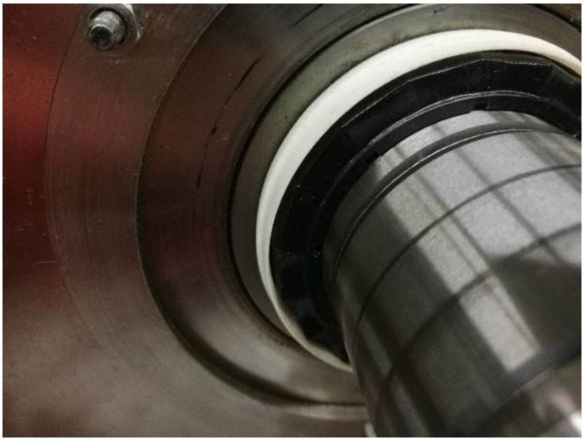

Figure 11 Assembled seal after test

5 Summary and Conclusion

The paper presents an advanced design of an axial acting seal. This proposed design shows several features to improve the lifetime under poor lubrication and accelerated velocities. Compared to radial oil seals the sealing element is rotating on the shaft and must be balanced to avoid unwanted vibrations while radial acting seals generate a high loss.

One notable advantage of the design is the adjustable torque or rather loss curve depending on the materials density and axial pretension. In addition, the paper shows a mathematical approach to estimate the leakage of a rotating sealing element for poor lubrication.

Furthermore, the first test with the seal shows a good behavior in different rpm areas and the spatial structures are reducing the load in the contact area. In addition, the simulation-based prediction and measured torque are showing a good accordance for $\mu=0.2$.

Looking ahead, it is necessary to carry out additional tests to determine the limits of the design. Also, the production is complex due to the multicomponent molding process and assembly of the sealing ring. Therefore, an updated design to avoid an additional assembly is conceivable.

6 Nomenclature

Variable	*Description*	*Unit*
μ	Coefficient of friction	[-]
D	Diameter	[m]
b	Contact width	[m]
p	Pressure / Contact pressure	[N/m²]
K	Pressure gradient	[N/m³]
M	Torque	[Nm]
η	Viscosity	[Pa*s]
P	Frictional power loss	[W]
ρ	Density	[kg/m³]
T	Temperature	[K]
u_r, u_φ, u_z	Components of fluid flow in cylinder coordinates	[m/s]
ξ	Scale factor to determine pressure reduction	[-]
v	Velocity	[m/s]
$\dot{V}$	Leakage volume flow	[m³/s]
ω	Angular velocity	

7 References

/1/	Arora, A. et al, Why Electric Cars Can't Come Fast Enough, Boston Consulting Group, https://www.bcg.com/publications/2021/why-evs-need-to-accelerate-their-market-penetration visited on 07.04.2022
/2/	Zapf, M. et al, *Cost-efficient and sustainable automotive Original German title Kosteneffiziente und nachhaltige Automobile,* ISBN 978-3-658-33251-8, Springer, Berlin, Germany, 2019
/3/	Müller, H. K., Nau, B. S., *Fluid Sealing Technology. Principles and Applications,* ISBN 978-0824799694, Marcel Dekker, Inc., New York, Basel, Hong Kong, 1998.
/4/	Engelke, T., *Einfluss der Elastomer-Schmierstoff-Kombination auf das Betriebsverhalten von Radialwellendichtringen*, https://doi.org/10.15488/7613, Dissertation, Hannover, Germany 2011
/5/	N, N., *Handbuch Insect*, https://insect.ima.uni-stuttgart.de/manual/Handbuch.pdf visited on 19.04.2022
/6/	Jordan, H., Wilke, M., *Eine neue Interpretation der elastomeren Kontaktdichtungen (RWDR) zur Steigerung der Leistungsfähigkeit*, In: 20th International Sealing Conference Stuttgart 2018, Stuttgart, Germany, pp. 245-252, October 12-13, 2018.

/7/	N, N., *Rotary Seals – product catalog*, Trelleborg Sealing Solutions, Stuttgart, Germany, 2018.
/8/	L.D. Landau, E.M. Lifschitz: Theoretical Physics. Part VI: *Hydrodynamics. Original German title: Lehrbuch der theoretischen Physik. Teil VI: Hydrodynamik*., ISBN 978-3808555545, Verlag Harri Deutsch, 5th edition, Frankfurt am Main, 2007
/9/	J. Spurk, N. Aksel: *Fluid Mechanics. Introduction to the Theory of Flow. Original German title: Strömungslehre. Einführung in der Theorie der Strömungen*., ISBN 978-3642131424, Springer, 8th edition, Berlin, 2010